We are IntechOpen, the world's leading publisher of Open Access books
Built by scientists, for scientists

6,900
Open access books available

185,000
International authors and editors

200M
Downloads

154
Countries delivered to

Our authors are among the

TOP 1%
most cited scientists

12.2%
Contributors from top 500 universities

CLARIVATE ANALYTICS
BOOK CITATION INDEX
INDEXED

WEB OF SCIENCE™

Selection of our books indexed in the Book Citation Index
in Web of Science™ Core Collection (BKCI)

Interested in publishing with us?
Contact book.department@intechopen.com

Numbers displayed above are based on latest data collected.
For more information visit www.intechopen.com

An Adaptive Neuro-Fuzzy Strategy for a Wireless Coded Power Control in Doubly-Fed Induction Aerogenerators

I. R. S. Casella, A. J. Sguarezi Filho, C. E. Capovilla,
J. L. Azcue and E. Ruppert

Additional information is available at the end of the chapter

1. Introduction

Renewable energy systems and specially wind energy have attracted governmental interests in opposition to energy sources that increase CO_2 emissions and cause enormous environmental impact. Recently, the concept of smart grid has been applied to power plants to enable and optimize the generation of energy by efficiently combining wind, solar and tidal. Moreover, the efforts for consolidation and implementation of this new concept through wind energy systems have attracted great interest from the technical community and has been the focus of several recent scientific works [1–3].

Smart grids are an evolution of conventional power grids to optimally manage the relationship between energy supply and demand in electrical systems to overcome the actual problem of contingency of energy of the modern world. They employ an interactive framework composed by integrated communication networks with real time monitoring, control and automatic intervention capability to use more efficiently the infrastructure of generation, transmission and distribution of energy.

Advances in wind power technology have greatly improved its system integration with smart grid, however, there are still some unsolved challenges in expanding its use. Due to the usual variations of the wind speed, its utilization entails undesirable fluctuations in the generated power that, if not compensated in real time, can lead to frequency imbalance and disturbance in the stability of the electrical system. Although smart grid can minimize this problem through a more precise demand response for load control and dispatch of other generation

resources, it is still necessary to employ variable speed aerogenerators and a precise power control system to guarantee stability and maximum power generation.

Among the existing aerogenerators, Doubly-Fed Induction Generators (DFIG) are the most widely employed in wind power systems [4] due to their interesting main characteristics as, for instance, the ability to operate at variable speed and the capacity to control the active and reactive power into four quadrants by means of field orientation [5, 6]. The precise power control of the aerogenerators is essential to maximize the generated power. The conventional Proportional-Integral (PI) [7] and Proportional-Integral-Derivative (PID) [8, 9] have been widely used as the core of different power control systems due to their simplicity of implementation. However, the design of these fixed gain control systems is very cumbersome, since it depends on the exact mathematical model of the generator. Also, they are very sensitive to disturbances, parameter variations and system nonlinearities.

On the other hand, the design of intelligent control systems based on Computational Intelligence (CI) does not require the exact mathematical model of the generator. Among of the CI techniques, Fuzzy Logic (FL) and Artificial Neural Networks (ANN) appear as powerful options for identification and control of nonlinear dynamic systems as power control systems. However, each of these intelligent techniques has its own drawbacks which restrict its use. For instance, FL suffers from some limitations as the appropriate selection of Membership Functions (MF), the adequate selection of fuzzy rules and, furthermore, how to adjust both of them to achieve the best performance. ANN have also some limitations as their black-box nature, the selection of the best structure and size, and the considerable training time to solve a specific problem. In order to overcome these problems, it is possible to use a hybrid neuro-fuzzy system [10] that can combine the learning capability of ANN with the knowledge representation of FL based on rules. One of the most widely used neuro-fuzzy system is the Adaptive Neural Fuzzy Inference System (ANFIS), proposed by [11]. It can use a hybrid learning procedure to construct an input-output mapping based on both human-knowledge as fuzzy rules and approximate MF from the corresponding input-output data pairs as ANN learning.

Another very important issue in the deployment of smart grids is the application of a modern telecommunications system to guarantee an effective monitoring and control of the grid. Nevertheless, its development and operability require a fairly complex infrastructure and present several non-trivial questions due to the convergence of different areas of knowledge and design aspects. In this way, the wireless transmission appears as an interesting solution for presenting many benefits such as low cost of development, expansion facilities, possibility of using the technologies currently applied in mobile telephone systems, flexibility of use, and distributed management. However, the employment of wireless technologies for transmitting power control signals may cause apprehension due to the possibility of the occurrence of errors in the transmission process that can cause serious problems to the generators and, consequentially, to the energy system. Such behavior is different from what usually happens in telecommunications systems designed to voice and data transmissions, where small errors can be detected, initiate requests for retransmission (generating delays) or even, in some cases, be ignored without any significant impact to the network. It is worth noting that there are some works in the scientific literature referencing the application of wireless technology for monitoring wind energy systems [12, 13], but there has not been presented any deep research about the use of wireless technology for control applications in

these systems yet, making it difficult to estimate the real impact of its use or its advantages and difficulties.
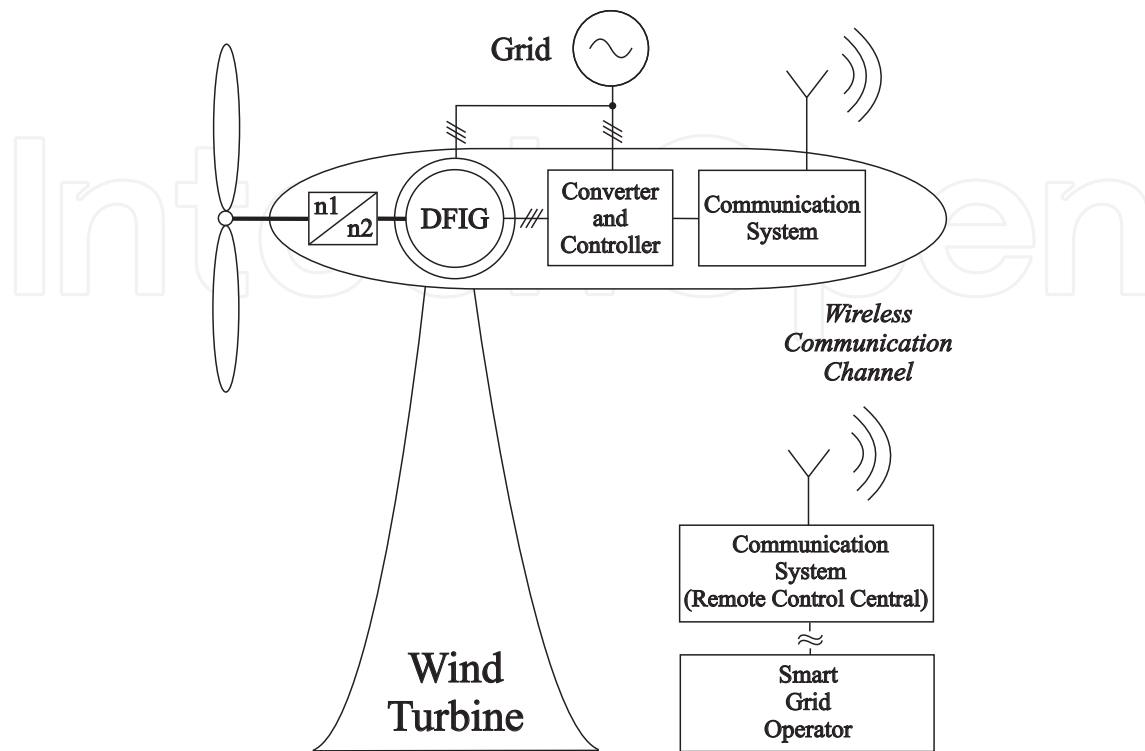

Figure 1. Wireless System Control Schematic.

Modern wireless digital communication techniques can be used to improve the robustness of the power control system and to minimize the mentioned problems through the application of Forward Error Correction (FEC) [14]. FEC is a coding technique used in all current digital wireless systems and it is essential to ensure the integrity of information, reducing significantly the Bit Error Rate (BER) and the latency of the information by adding controlled redundancy to the transmitted information [15]. In theory, the appropriate use of coding technology can offer the same reliability obtained by using fiber optic cables [16].

There are currently several different schemes of FEC that are used in commercial wireless communication systems [17], [18], [19–21]. Among them, LDPC is the one that presents the best performance and shows an excellent compromise between decoding complexity and performance [22, 23].The LDPC coding has recently been added to the IEEE 802.16e Standard, commonly known as Worldwide Interoperability for Microwave Access (WiMAX) for mobile applications [24].

In this context, this chapter will analyze the performance of a new wireless coded adaptive neuro-fuzzy power control system for variable speed wind DFIG, presented in Fig. 1. The system is based on a discrete dynamic mathematical model of the generator and uses the vector control technique to independently control the active and reactive power. The proposed adaptive neuro-fuzzy system is designed from an input and output data set collected from a DFIG with a deadbeat controller [25] operating at different conditions and considering the rotor current error as input. The wireless communication system, employed

to send the power reference signals to the DFIG controller, uses LDPC coding to reduce the transmission errors and the overall latency of the system. The performance of the system is investigated in a frequency flat fading scenario, to evaluate the real impact of the wireless transmission in the wind energy control system. It is noteworthy that the errors generated in the wireless transmission cannot be easily removed without using advanced FEC coding techniques similar to those presented in this work.

2. Doubly-Fed Induction Generator model

The DFIG model in synchronous dq reference frame can be mathematically represented by [26]:

$$\vec{v}_{1dq} = R_1\vec{i}_{1dq} + \frac{d\vec{\lambda}_{1dq}}{dt} + j\omega_1\vec{\lambda}_{1dq} \tag{1}$$

$$\vec{v}_{2dq} = R_2\vec{i}_{2dq} + \frac{d\vec{\lambda}_{2dq}}{dt} + j\left(\omega_1 - N_P\omega_{mec}\right)\vec{\lambda}_{2dq} \tag{2}$$

and the relationships between fluxes and currents are:

$$\vec{\lambda}_{1dq} = L_1\vec{i}_{1dq} + L_M\vec{i}_{2dq} \tag{3}$$

$$\vec{\lambda}_{2dq} = L_M\vec{i}_{1dq} + L_2\vec{i}_{2dq} \tag{4}$$

so, the active and reactive power are given by:

$$P = \frac{3}{2}\left(v_{1d}i_{1d} + v_{1q}i_{1q}\right) \tag{5}$$

$$Q = \frac{3}{2}\left(v_{1q}i_{1d} - v_{1d}i_{1q}\right) \tag{6}$$

The subscripts 1 and 2 represent the stator and rotor parameters, respectively; ω_1 represents the synchronous speed, ω_{mec} represents machine speed, R represents winding per phase electrical resistance, L and L_M represent the proper and the mutual inductances of windings, $\vec{v}$ represents voltage vector, and N_P represents the machine number of pair of poles.

The DFIG power control aims independent stator active P and reactive Q power control by means of a rotor current regulation. For this purpose, P and Q are represented as functions

of each individual rotor current. Using stator flux orientation, that decouples the dq axis, it has that $\lambda_{1d} = \lambda_1 = |\vec{\lambda}_{1dq}|$, thus, the equation (3) becomes:

$$i_{1d} = \frac{\lambda_1}{L_1} - \frac{L_M}{L_1} i_{2d} \tag{7}$$

$$i_{1q} = -\frac{L_M}{L_1} i_{2q} \tag{8}$$

Similarly, using stator flux oriented, the stator voltage becomes $v_{1d} = 0$ and $v_{1q} = v_1 = |\vec{v}_{1dq}|$. Hence, the active (5) and reactive (6) powers can be calculated by using equations (7) and (8):

$$P = -\frac{3}{2} v_1 \frac{L_M}{L_1} i_{2q} \tag{9}$$

$$Q = \frac{3}{2} v_1 \left(\frac{\lambda_1}{L_1} - \frac{L_M}{L_1} i_{2d} \right) \tag{10}$$

Thus, the rotor currents will reflect on the stator currents and on the active and reactive power of the stator, respectively. Consequently, this principle can be used to control the active and reactive power of the DFIG stator.

Thus, the rotor currents will reflect on the stator currents and the active and reactive power of the stator, respectively. Therefore, this principle can be used to control the active and reactive power of the DFIG.

3. Adaptive Neuro-Fuzzy Power Control

As mentioned before, an accurate power control system of the aerogenerators connected to the grid is essential to guarantee stability and maximum energy generation. In this way, ANFIS has been shown a powerful technique to control the nonlinear dynamic behavior of aerogenerators. Usually, it can use a hybrid learning procedure to construct an input-output mapping based on both human-knowledge as fuzzy rules and approximate MF from the stipulated input-output data pairs as ANN learning to precisely control the power generation.

3.1. ANFIS overview

An ANFIS is an adaptive network architecture whose overall input-output behavior is determined by the values of a collection of modifiable parameters [11, 27]. More specifically, the configuration of an adaptive network is composed by a set of nodes connected through directed links, where each node is a process unit that performs a static node function on its

incoming signals to generate a single node output and each link specifies the direction of the signal flow from one node to another.

The parameters of an adaptive network are distributed into the network nodes, so each node has a local parameter set. The union of these local parameter sets forms the network overall parameter set. If a node parameter set is non-empty, then its node function depends on the parameter values, and it is used a square to represent this kind of adaptive node. On the other hand, if a node has an empty parameter set, then its function is fixed and it is used a circle to denote this type of fixed node [11].

This technique offers a method for learning information about a given data set during the fuzzy modeling procedure in order to adjust the MF parameters that best control the associated fuzzy inference system (FIS) to obtain the desired behavior.

3.1.1. ANFIS Architecture

In order to describe the ANFIS architecture in more detail, it is considered in the following, without loss of generality, a system with two inputs x_1 and x_2 and one output y, based on a first-order Takagi-Sugeno fuzzy model [28] with the fuzzy rules expressed as:

$$\text{Rule 1}: \text{ If } x_1 \text{ is } A_1 \text{ and } x_2 \text{ is } B_1 \text{ then } f_1 = p_1 x_1 + q_1 x_2 + r_1 \tag{11}$$

$$\text{Rule 2}: \text{ If } x_1 \text{ is } A_2 \text{ and } x_2 \text{ is } B_2 \text{ then } f_2 = p_2 x_1 + q_2 x_2 + r_2 \tag{12}$$

The ANFIS network structure is composed by a set of units and connections arranged into five layers [11, 27, 29], as shown in Fig. 2, where the output of the ith node of the lth layer is denoted as $O_{l,i}$.
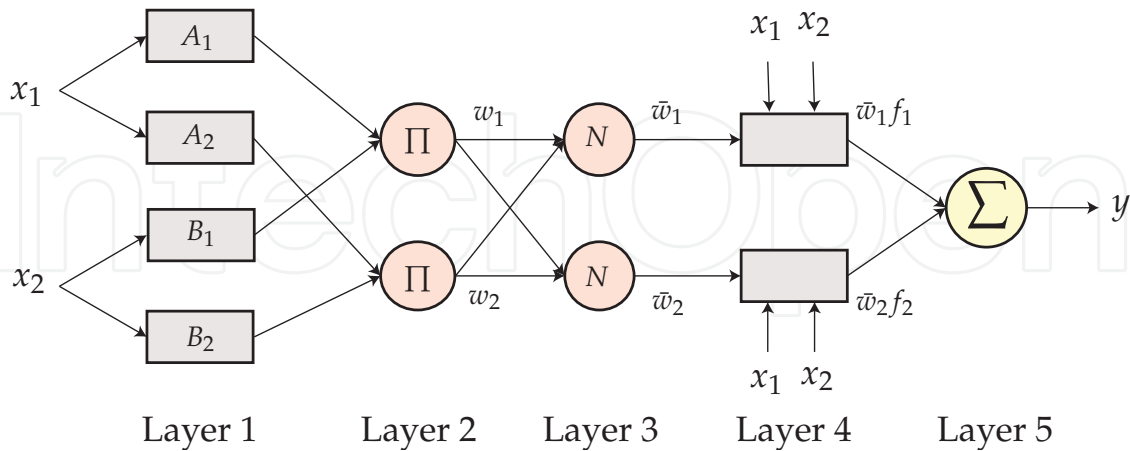

Figure 2. ANFIS Structure [11]

- Layer 1: Nodes in this layer are adaptive nodes and represent the membership grade of the inputs x_1 and x_2. Here, triangular or bell shaped MF [11] can be used. The parameters of this layer are called premise parameters and the nodes outputs are represented by:

$$O_{1,i} = \mu_{A_i}(x_1), \quad \text{for } i = 1, 2 \text{ or}$$
$$O_{1,i} = \mu_{B_{i-2}}(x_2), \quad \text{for } i = 3, 4 \tag{13}$$

where $\mu_{A_i}(x_1)$ and $\mu_{B_{i-2}}(x_2)$ are, respectively, the MF for the inputs x_1 and x_2.

- Layer 2: Each node in this layer, denoted as Π, is a non-adaptive node. This layer receives the input values x_1 and x_2 from the first layer and acts as a MF to represent the fuzzy sets of the respective input variables. Further, it computes the membership values that specify the degree to which the input values belongs to the fuzzy set. The nodes outputs are defined by the following product:

$$O_{2,i} = w_i = \mu_{A_i}(x_1) \cdot \mu_{B_i}(x_2), \quad \text{for } i = 1, 2 \tag{14}$$

- Layer 3: Each node in this layer, denoted as N, is a non-adaptive node that normalizes the weight functions obtained from layer Π. This layer is usually called as the rule layer since it determines the activation level of each rule. The nodes outputs are given by:

$$O_{3,i} = \bar{w}_i = \frac{w_i}{w_1 + w_2}, \quad \text{for } i = 1, 2 \tag{15}$$

- Layer 4: Every node i in this layer is an adaptive node. The parameters of this layer are called consequent parameters and the nodes outputs are expressed by:

$$O_{4,i} = \bar{w}_i f_i = \bar{w}_i (p_i x_1 + q_i x_2 + r_i), \quad \text{for } i = 1, 2 \tag{16}$$

where $\bar{w}_i$ is the output of layer 3 and $\{p_i, q_i, r_i\}$ are the consequent parameters set.

- Layer 5: This layer, denoted by Σ, is non-adaptive and produces the output function by adding all inputs from the previous layers and transforming the fuzzy classification results into a crisp value, as expressed by:

$$O_{5,1} = \sum_i \bar{w}_i f_i = \frac{\sum_i w_i f_i}{\sum_i w_i} \tag{17}$$

3.1.2. Hybrid Learning Algorithm

The learning process can update the MF parameters by a hybrid learning procedure [29] composed by the Least Squares (LS) method, which is applied for tuning the linear output MF parameters, and the Backpropagation (BP) method, which is employed for tuning the nonlinear input MF parameters [30].

In the forward pass, LS estimates the consequent parameters, keeping the premise parameter fixed, and in the backward pass, the premise parameters are obtained by BP, keeping the

consequent parameter fixed. When the values of the premise parameters are fixed, the overall output can be expressed as a linear combination of the consequent parameters.

Thus, considering the general LS approach, the output y of a given system to an input $\mathbf{x}$ can be represented by the following linearly parameterized equation:

$$y = \theta_1 f_1(\mathbf{x}) + \theta_2 f_2(\mathbf{x}) + \cdots + \theta_{N_i} f_{N_i}(\mathbf{x}) \tag{18}$$

where $\mathbf{x}$ is the input vector of the model with dimension N_x, f_i are known functions of $\mathbf{x}$, θ_i are the unknown parameters to be optimized and $i = 1, \cdots, N_i$.

Usually, to identify the unknown parameters, a training set of data pairs $(\mathbf{u}_m, v_m)$ is employed, where $\mathbf{u}$ is a vector with dimension N_x and $m = 1, \cdots, N_m$. Substituting each data pair into equation (18) yields the following set of N_m linear equations:

$$\begin{array}{ccccccc}
f_1(\mathbf{u}_1)\theta_1 & + & f_2(\mathbf{u}_1)\theta_2 & + & \cdots & + & f_{N_i}(\mathbf{u}_1)\theta_{N_i} & = & v_1 \\
\vdots & & \vdots & & & & \vdots & & \vdots \\
f_1(\mathbf{u}_{N_m})\theta_1 & + & f_2(\mathbf{u}_{N_m})\theta_2 & + & \cdots & + & f_{N_i}(\mathbf{u}_{N_m})\theta_{N_i} & = & v_{N_m}
\end{array} \tag{19}$$

These equations can also be expressed through the following vector representation:

$$\mathbf{A} \times \boldsymbol{\theta} = \mathbf{v} \tag{20}$$

where $\mathbf{A}$ is a (N_m) by (N_i) matrix:

$$\mathbf{A} = \begin{bmatrix} f_1(\mathbf{u}_1) & \cdots & f_{N_i}(\mathbf{u}_1) \\ \vdots & \ddots & \vdots \\ f_1(\mathbf{u}_{N_m}) & \cdots & f_{N_i}(\mathbf{u}_{N_m}) \end{bmatrix} \tag{21}$$

$\boldsymbol{\theta}$ is the (N_i) by (1) vector of unknown parameter:

$$\boldsymbol{\theta} = \begin{bmatrix} \theta_1 \\ \vdots \\ \theta_{N_i} \end{bmatrix} \tag{22}$$

and $\mathbf{v}$ is the (N_m) by (1) output vector:

$$\mathbf{v} = \begin{bmatrix} v_1 \\ \vdots \\ v_{N_m} \end{bmatrix} \tag{23}$$

Usually, $N_m > N_i$ and, instead of directly obtaining a solution for equation (20), an error vector $\mathbf{e}$ is introduced, resulting in the following equation:

$$\mathbf{A} \times \boldsymbol{\theta} + \mathbf{e} = \mathbf{v} \tag{24}$$

Whose solution $\boldsymbol{\theta} = \hat{\boldsymbol{\theta}}$ is obtained by minimizing the sum of the squared error:

$$\ell(\boldsymbol{\theta}) = \sum_{m=1}^{N_m} \left(v_m - \mathbf{a}_m^T \times \boldsymbol{\theta} \right)^2 = \mathbf{e}^T \times \mathbf{e} \tag{25}$$

where $\ell(\boldsymbol{\theta})$ is the objective function, $\mathbf{a}_m^T$ is the mth row vector of $\mathbf{A}$, $\mathbf{e} = \mathbf{v} - \mathbf{A} \times \boldsymbol{\theta}$ is the error vector produced by a specific choice of $\boldsymbol{\theta}$ and $()^T$ is the transpose operation.

The squared error in equation (25) is minimized when $\boldsymbol{\theta} = \hat{\boldsymbol{\theta}}$, where $\hat{\boldsymbol{\theta}}$ is obtained through a LS estimator that satisfies the following normal equation:

$$\left(\mathbf{A}^T \times \mathbf{A} \right) \times \boldsymbol{\theta} = \mathbf{A}^T \times \mathbf{v} \tag{26}$$

If $\mathbf{A}^T \times \mathbf{A}$ is non-singular, the LS solution $\hat{\boldsymbol{\theta}}$ can be obtained by:

$$\hat{\boldsymbol{\theta}} = \left(\mathbf{A}^T \times \mathbf{A} \right)^{-1} \times \mathbf{A}^T \times \mathbf{v} \tag{27}$$

where $\left(\mathbf{A}^T \times \mathbf{A} \right)^{-1} \times \mathbf{A}^T$ is the pseudo-inverse of $\mathbf{A}$ [30] and $()^{-1}$ is the inverse operation.

The LS solution is computationally very expensive, mainly for vectorial inputs, since it requires matrix inversion. Moreover, it can become ill-conditioned if $\mathbf{A}^T \times \mathbf{A}$ becomes singular. Thus, in practice, a recursive LS (RLS) algorithm can usually be employed [11, 29, 30].

In the backward pass, the premise parameters are estimated iteratively by a modified BP procedure that employs the Gradient Descent (GD) algorithm along with the chain rule to find the minimum of the error function in the weight space [29]. Considering a feed-forward adaptive network with N_L layers and N_i^l nodes in the lth layer, the output $O_{l,i}$ of the ith node of the lth layer can be represented by:

$$O_{l,i} = f_{l,i}\left(O_{l-1,1}, \cdots, O_{l-1,N_i^{l-1}}, \xi_{l,i}^1, \xi_{l,i}^2, \cdots, \xi_{l,i}^{N_\xi}\right) \tag{28}$$

where $f_{l,i}()$ is the node function of the ith node of the lth layer and $\xi_{l,i}^1, \xi_{l,i}^2, \cdots, \xi_{l,i}^{N_\xi}$ are the parameters associated with this specific node.

Assuming that the training data set has N_m terms, a measure of error at the output layer L corresponding to the mth term of the training set, where $1 \leq m \leq N_m$, can be defined as [11, 27, 29]:

$$\ell_m = \sum_{i=1}^{N_i^L} \left(v_m^i - O_{L,i}^m\right)^2 \tag{29}$$

where v_m^i is the mth desired output for the ith node of the output layer (L^{th} layer) and $O_{L,i}^m$ is the actual output of the ith node of the output layer produced by applying the mth training input vector to the network.

In this way, the main task of this step is to employ the GD algorithm to minimize the total measure of error defined as:

$$\ell_{total} = \sum_{m=1}^{N_m} \ell_m \tag{30}$$

In order to compute the gradient vector of the parameters, a form of the derivative information has to be passed backward, layer by layer, from the output layer to the input layer. This procedure is called BP because the gradient is obtained sequentially from the output layer to the input layer.

The corresponding error signal $e_{l,i}$ can be defined by the ordered derivative [31] of ℓ_m with respect to the output of the ith node of the lth layer:

$$e_{l,i}^m = \frac{\partial^+ \ell_m}{\partial O_{l,i}^m} \tag{31}$$

Particularly, for the output layer L, the error signal can be represented by the following simplified expression:

$$e_{L,i}^m = -2\left(v_m^i - O_{L,i}^m\right) \tag{32}$$

For the internal i^{th} node at the lth layer, the error signal can be derived iteratively by the following chain rule [11, 29]:

$$e_{l,i}^m = \sum_{m=1}^{N_i^{l+1}} \frac{\partial^+ \ell_m}{\partial O_{l+1,i}^m} \frac{\partial f_{l+1,m}}{\partial O_{l,i}^m}$$

$$= \sum_{m=1}^{N_i^{l+1}} e_{l+1,i}^m \frac{\partial f_{l+1,m}}{\partial O_{l,i}^m} \tag{33}$$

where $1 \le l \le N_L - 1$ and $N_L = 5$ for the considered ANFIS model.

As the consequent parameters are fixed in the backward pass, the gradient vector can be defined as the derivative of the error measure with respect to the node parameters of the first layer $\varsigma_{1,i}$. The gradient vector elements corresponding to the ith node of 1st layer are given by:

$$\frac{\partial^+ \ell_m}{\partial \varsigma_{1,i}} = \frac{\partial^+ \ell_m}{\partial v_{1,i}} \frac{\partial f_{1,i}}{\partial \varsigma_{1,i}}$$

$$= e_{1,i} \frac{\partial f_{1,i}}{\partial \varsigma_{1,i}} \tag{34}$$

The derivative of the total error measure ℓ_{total} with respect to $\varsigma_{1,i}$ is given by:

$$\frac{\partial^+ \ell_{total}}{\partial \varsigma_{1,i}} = \sum_{m=1}^{N_m} \frac{\partial^+ \ell_m}{\partial \varsigma_{1,i}} \tag{35}$$

Accordingly, the parameter $\varsigma_{1,i}$ can be updated using the following expression:

$$\Delta \varsigma_{1,i} = -\eta \frac{\partial^+ \ell_{total}}{\partial \varsigma_{1,i}} \tag{36}$$

where η is the learning rate [11, 29].

The parameter $\varsigma_{1,i}$ can be updated employing the following recursive expression:

$$\varsigma_{1,i}^{new} = \varsigma_{1,i}^{old} + \Delta \varsigma_{1,i}$$

$$= \varsigma_{1,i}^{old} - \eta \frac{\partial^+ \ell_{total}}{\partial \varsigma_{1,i}} \tag{37}$$

In this type of learning procedure, the MF update occurs only after the whole set of training data pair is introduced. This process of introduction of the whole set of training data pairs is called epoch.

3.2. Proposed Adaptive Neuro-Fuzzy Power Control

The proposed adaptive neuro-fuzzy power control system, shown in Fig. 3, is composed by two ANFIS controllers based on a first-order Takagi-Sugeno fuzzy model [28] with one input and one output. The first controller has ε_{2q} as input and v_{2q} as output, and the second controller has ε_{2d} and v_{2d} as input and output, respectively, where $\varepsilon_{2q} = i_{2q_{ref}} - i_{2q}$ and $\varepsilon_{2d} = i_{2d_{ref}} - i_{2d}$.
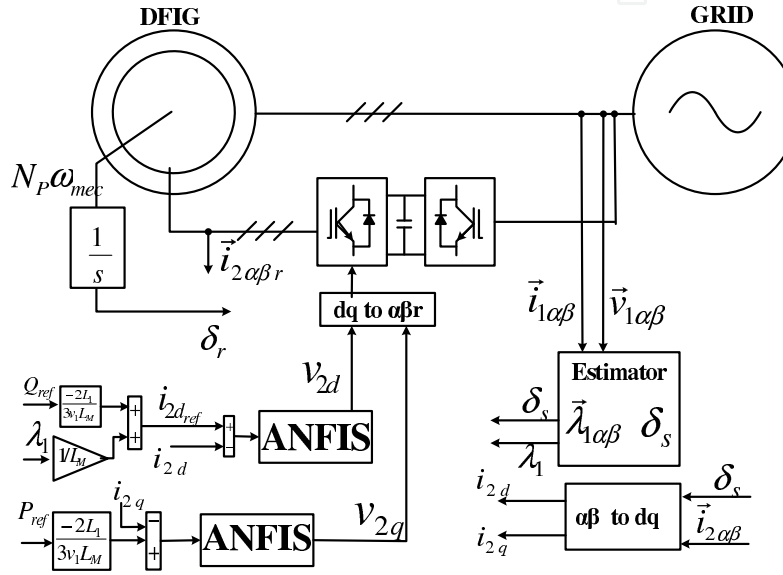

Figure 3. Neuro-Fuzzy DFIG Power Control.

Differently from what has been presented in the literature [10], the ANFIS controller employs just the rotor current error as input and it is designed from an input and output data set collected from a DFIG with a deadbeat controller [25] operating at different conditions.

In Fig. 4, it is shown a simplified representation of the substitution that was made in this work with the purpose of illustrating that the designed ANFIS presents the same behavior of a deadbeat controller.
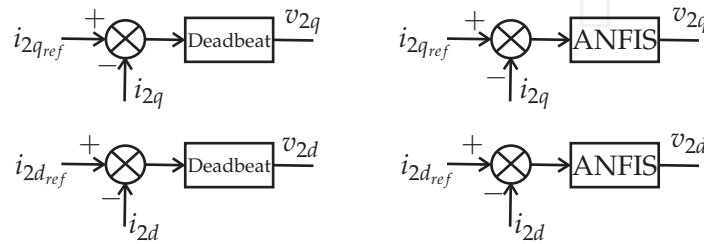

Figure 4. ANFIS Controller.

The tests used in this work for collect data set training are similar to the ones used in [10]:

- Operation at different wind speed profiles;
- Operation at different ramp increments in wind speed;
- Operation at different step increments in wind speed;
- Operation during voltage sag conditions.

The grid partition method is chosen to design the fuzzy controller structure, which usually involves just some few state variables as inputs to the controller. A generalized bell MF with parameters a, b, c, besides the input u, has been considered:

$$bell(u, a, b, c) = \frac{1}{1 + |\frac{u-c}{a}|^{2b}}$$

(38)

where, the parameter b is usually positive.

The desired generalized bell MF can be obtained by a proper selection of the parameter set $\{a, b, c\}$. Specifically, we can adjust c and a to vary, respectively, the center and width of the MF and then use b to control the slopes at the crossover points [27].

To calculate the numerical value resulting from the activated rules, it was used the weighted average method for defuzzification. Thus, if the *direct* and *quadrature* voltage components are calculated according to the ANFIS controller and are applied to the generator, then the active and reactive power convergence to their respective commanded values will occur in a few sampling intervals. The desired rotor voltage in the rotor reference frame $(\delta_s - \delta_r)$ generates switching signals for the rotor side using either space vector modulation.

4. Flux estimation

For work properly, the ANFIS controller requires the estimation of stator flux, stator position and angle between stator and rotor flux.

The stator flux $\vec{\lambda}_{1\alpha\beta}$ in stationary reference frame can be estimated by:

$$\vec{\lambda}_{1\alpha\beta} = \int \left(\vec{v}_{1\alpha\beta} - R_1 \vec{i}_{1\alpha\beta} \right) dt$$

(39)

The stator flux position can be obtained by using equation (39) as:

$$\delta_s = \arctan\left(\frac{\lambda_{1\beta}}{\lambda_{1\alpha}}\right)$$

(40)

And the angle between stator and rotor flux is given by:

$$\delta_s - \delta_r = \int \omega_{sl} dt$$

(41)

5. Wireless Coded Communication System

The wireless communication system, shown in Fig. 5, is responsible for transmitting the power references from the remote control unit to the ANFIS controller and it uses Quaternary Phase Shift Keying (QPSK) modulation and LDPC coding [18, 32, 33] to improve system performance and reliability.
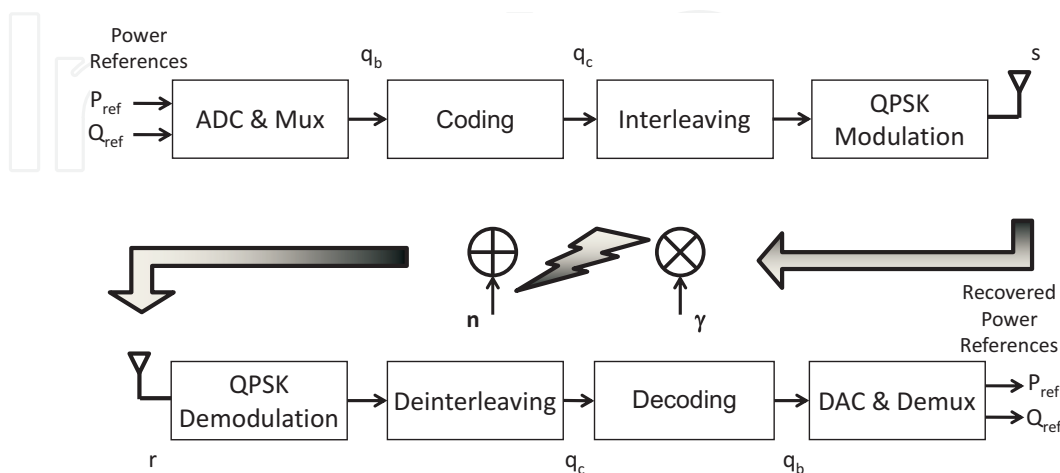

Figure 5. Wireless Coding Communication Diagram.

LDPC are (N_c, N_b) binary linear block codes that have a sparse parity-check matrix **H** that can be described in terms of a Tanner graph [34], where each bit in the codeword corresponds to a variable node and each parity-check equation corresponds to a check node. A check node j is connected to a variable node k whenever the element $h_{j,k}$ in **H** is equal to 1 [18, 34].

Extended Irregular Repeat Accumulate (eIRA) codes [35–39] are a special subclass of LDPC codes that improve the systematic encoding process and generate good irregular LDPC codes for high code rate applications. The eIRA parity-check matrix can be represented by $\mathbf{H} = [\mathbf{H}_1 \ \mathbf{H}_2]$, where $\mathbf{H}_1$ is a sparse (N_z) by (N_c) matrix, that can be constructed irregularly by density evolution according to optimal weight distribution [38], and $\mathbf{H}_2$ is the (N_z) by (N_z) dual-diagonal square matrix given by:

$$\mathbf{H}_2 = \begin{bmatrix} 1 & & & & \\ 1 & 1 & & & \\ & 1 & \ddots & & \\ & & \ddots & 1 & \\ & & & 1 & 1 \end{bmatrix} \tag{42}$$

where N_b is the number of control bits, N_c is the number of coded bits and N_z is the number of parity bits.

Given the constraint imposed on the **H** matrix, the generator matrix can be represented in the systematic form by the (N_b) by (N_c) matrix:

$$\mathbf{G} = [\mathbf{I} \ \mathbf{\Psi}] \tag{43}$$

where $\mathbf{I}$ is the identity matrix, $\mathbf{\Psi} = \mathbf{H}_1^T \times \mathbf{H}_2^{-T}$, $()^{-T}$ is the inverse transpose operation, and $\mathbf{H}_2^{-T}$ is the upper triangular matrix given by:

$$\mathbf{H}_2^{-T} = \begin{bmatrix} 1 & 1 & 1 & \cdots & 1 & 1 \\ & 1 & 1 & \cdots & 1 & 1 \\ & & 1 & & 1 & 1 \\ & & & \ddots & \vdots & \vdots \\ & & & & 1 & 1 \\ & & & & & 1 \end{bmatrix} \tag{44}$$

The encoding process can be accomplished by first multiplying the control information vector $\mathbf{q}_b = \begin{bmatrix} q_{b,1} & \cdots & q_{b,N_b} \end{bmatrix}^T$ by the sparse matrix $\mathbf{H}_1^T$ and then differentially encoding this partial result to obtain the parity bits. The systematic codeword vector $\mathbf{q}_c = \begin{bmatrix} q_{c,1} & \cdots & q_{c,N_c} \end{bmatrix}^T$ can be simply obtained by combining the control information and the parity bits.

In the transmission process, for each transmitted frame, the codeword vector is interleaved and mapped to QPSK symbols by using Gray coding [15], resulting in the symbol vector $\mathbf{s} = \begin{bmatrix} s_1 & \cdots & s_{N_s} \end{bmatrix}^T$, where N_s is the number of transmitted coded control symbols. Afterward, the coded symbols are filtered, upconverted and transmitted by the wireless fading channel.

Assuming that the channel variations are slow enough that intersymbol interferences (ISI) can be neglect, the fading channel can be modeled as a sequence of zero-mean complex Gaussian random variables with autocorrelation function [15, 40]:

$$R_h(\tau) = J_0(2\pi f_D T_s) \tag{45}$$

where $J_0()$ is the $zero^{th}$ order Bessel function, T_s is the signaling time and f_D is the Doppler spread.

Thus, in the receive process, the complex low-pass equivalent discrete-time received signal can be represented by [15]:

$$\mathbf{r} = \boldsymbol{\gamma} \cdot \mathbf{s} + \mathbf{n} \tag{46}$$

where $\mathbf{r} = \begin{bmatrix} r_1 & \cdots & r_{N_s} \end{bmatrix}^T$ is the received signal vector, $\boldsymbol{\gamma} = \begin{bmatrix} \gamma_1 & \cdots & \gamma_{N_s} \end{bmatrix}^T$ is the vector of complex coefficients of the channel and $\mathbf{n} = \begin{bmatrix} n_1 & \cdots & n_{N_s} \end{bmatrix}^T$ is the Additive White Gaussian

Noise (AWGN) vector. Note that the above vector multiplication is performed element by element.

Once the transmitted vector **s** is estimated, considering perfect channel estimation, the transmitted control bits can be recovered by performing symbol demapping, code deinterleaving and bit decoding. Bit decoding can be accomplished by a message passing algorithm [23, 41–43] based on the Maximum A Posteriori (MAP) criterion [18], that exchanges soft-information iteratively between the variable and check nodes.

The exchanged messages can be represented by the following Log-Likelihood Ratio (LLR):

$$L_{c_k} = \log \left[\frac{p(\mathbf{q}_{c,k} = 0 | \mathbf{d})}{p(\mathbf{q}_{c,k} = 1 | \mathbf{d})} \right] \tag{47}$$

where, **d** is the vector of coded bits obtained by the processes of demodulation and deinterleaving.

The LLR message from the jth check node to the kth variable node is given by [37]:

$$L_{r_{j,k}} = 2 \operatorname{atanh} \left[\prod_{k' \in V_{j \setminus k}} \tanh \left(\frac{L_{q_{k',j}}}{2} \right) \right] \tag{48}$$

On the other hand, the LLR message from the kth variable node to the jth check node is obtained by:

$$L_{q_{k,j}} = L_{c_k} + \sum_{j' \in C_{k \setminus j}} L_{r_{j',k}} \tag{49}$$

And the LLR for the kth code bit can be represented by:

$$L_{Q_k} = L_{c_k} + \sum_{j \in C_k} L_{r_{j,k}} \tag{50}$$

where the set V_j contains the variable nodes connected to the jth check node and the set C_k contains the check nodes connected to the kth variable node. $V_{j \setminus k}$ is the set V_j without the kth element, and $C_{k \setminus j}$ is the set C_k without the jth element.

At the end of each iteration, L_{Q_k} provides an updated estimate of the a posteriori LLR of the transmitted coded bit $q_{c,k}$. If $L_{Q_k} > 0$, then $\hat{q}_{c,k} = 1$, else $\hat{q}_{c,k} = 0$.

6. Performance of the Wireless Power Control System

In the presented simulations, the sampling time is of 5×10^{-5}s and the active and reactive power references are step changed, respectively, from -100 to -120 kW and from 60 to 0 kvar at 1.25s. At 1.5s, the references also are step changed from -120 to -60 kW and from 0 to -40 kvar. Again, at 1.75s, the references are step changed from -60 to -100 kW and from -40 to -60 kvar. These references are the inputs of the wireless coded power control shown in Fig. 5. The nominal power at each instant of time is calculated by means of the turbine parameters, presented in the Appendix, and the speed of the wind, monitored by the remote control unit (that can also be obtained directly from the turbine and sent to the remote control unit).

The wireless control system is evaluated in a frequency flat fading Rayleigh channel with a Doppler spread of 180 Hz. The employed LDPC coding scheme is the (64800, 32400) eIRA code specified in [44] and an ordinary Convolution Coding (CC) scheme with a (171, 133) generator polynomial with constrain length of 7 is used as a reference of performance [18]. Both schemes have code rate of 1/2 and employ a random interleaving of length 64,800. For simplicity, the number of iterations in the LDPC decoding is limited to 25. The bit duration is 16×10^{-5} s and each transmitted frame is composed by 32,400 QPSK coded symbols.

The training process of the adaptive neuro-fuzzy power control strategy employed in this work considered a maximum of 5,000 epochs and an error tolerance of 0.0001.

In Fig. 6 and 7, the step response of the active and reactive power and of the rotor currents of the wireless controller using CC scheme are presented, respectively, considering an E_b/N_0 of 10 dB.
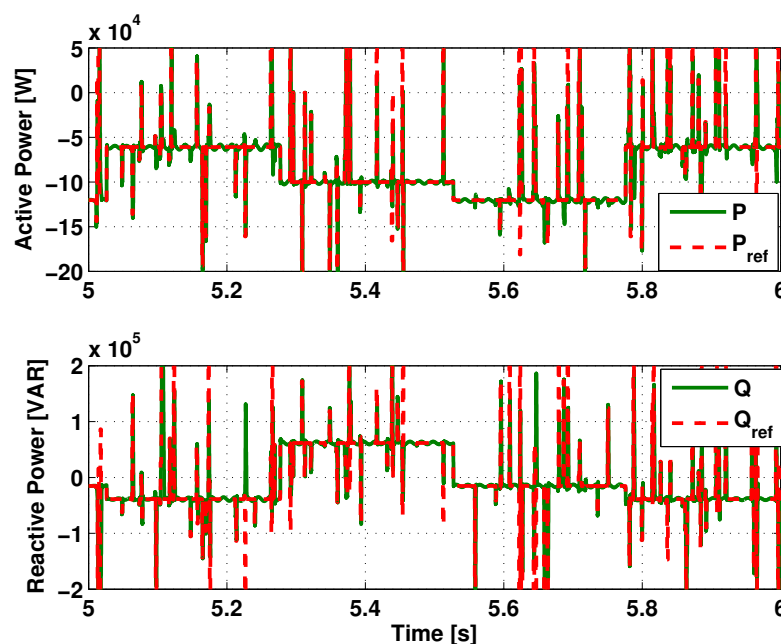

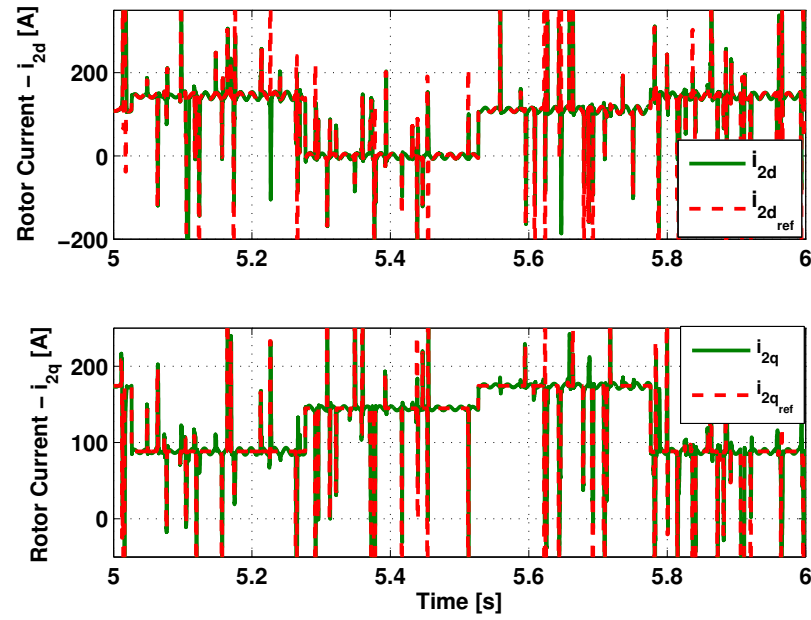**Figure 6.** Step Response of Active and Reactive Power using CC in a Flat Fading Channel.

Figure 7. Step Response of Rotor Current $\vec{i}_{2_{dq}}$ using CC in a Flat Fading Channel.

The spikes presented in the responses of the system occur due to the errors in the wireless communication caused by the fading channel, even with the use of a very efficient error correction CC scheme. It can be observed that several of these spikes, presented in the recovered reference signals, are followed by the controller.
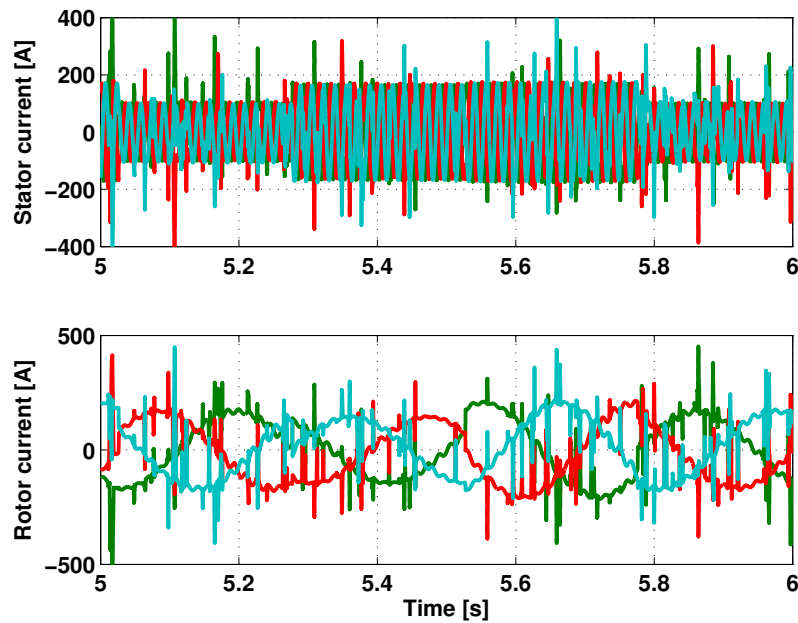

Figure 8. Stator and Rotor Currents using CC in a Flat Fading Channel.

These errors in the control system can permanently damage the aerogenerator or even cause a loss of system efficiency, since the machine will not generate its maximum power track at that moment. Additionally, they generate undesirable harmonic components to the power grid. As shown in Fig. 8, the damages can occur due to the high values of $\frac{di}{dt}$ that can completely deteriorate the Insulated Gate Bipolar Transistors (IGBTs) and, consequently, cause short circuits in rotor and/or stator of the generator through the power converter.
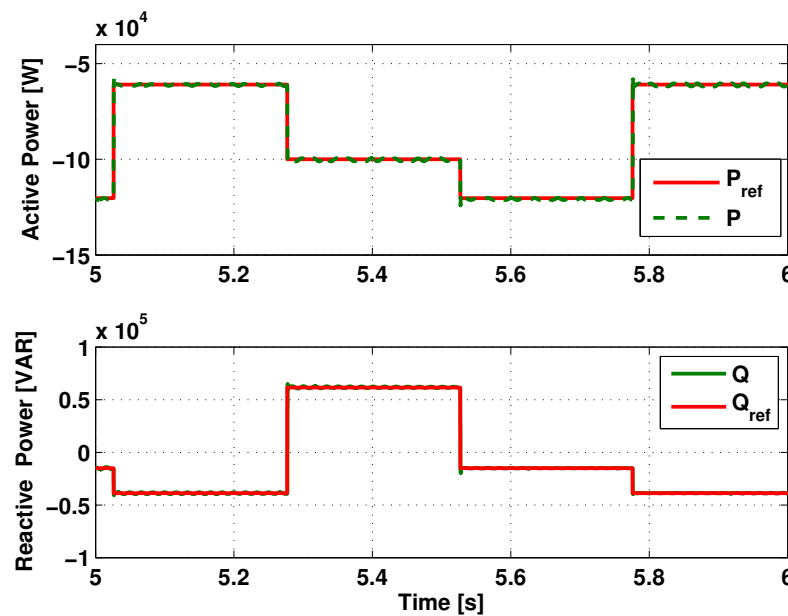

Figure 9. Step Response of Active and Reactive Power using LDPC in a Flat Fading Channel.

In this way, it turns out the necessity of employing a wireless coded control system capable of minimizing the occurrence of these spikes arising from errors caused by the channel distortions. With this finality, it is highlighted the proposal of using a more robust wireless neuro-fuzzy power control system based on LDPC coding.

In Fig. 9 and 10, the step response of the active and reactive power and of the rotor currents of the wireless controller using the LDPC scheme are presented, respectively, considering an E_b/N_0 of 10 dB. The satisfactory performance of the wireless control system can be seen due to the fact the references were perfectly followed by the controller and the inexistence of destructive spikes caused by errors in the wireless transmission system. Additionally, these good functionalities are shown in Fig. 11, where the stator currents present expected waveforms.
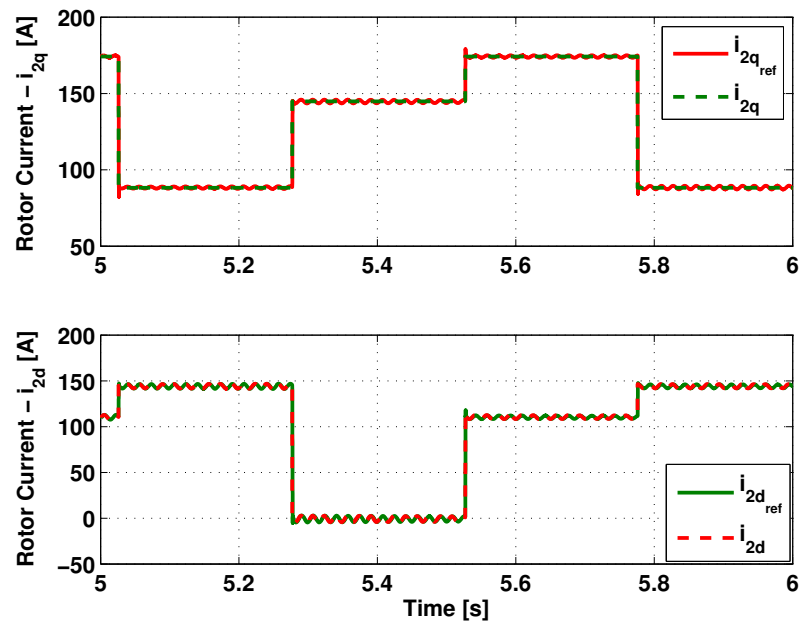
Figure 10. Step Response of Rotor Current $\vec{i}_{2_{dq}}$ using LDPC in a Flat Fading Channel.
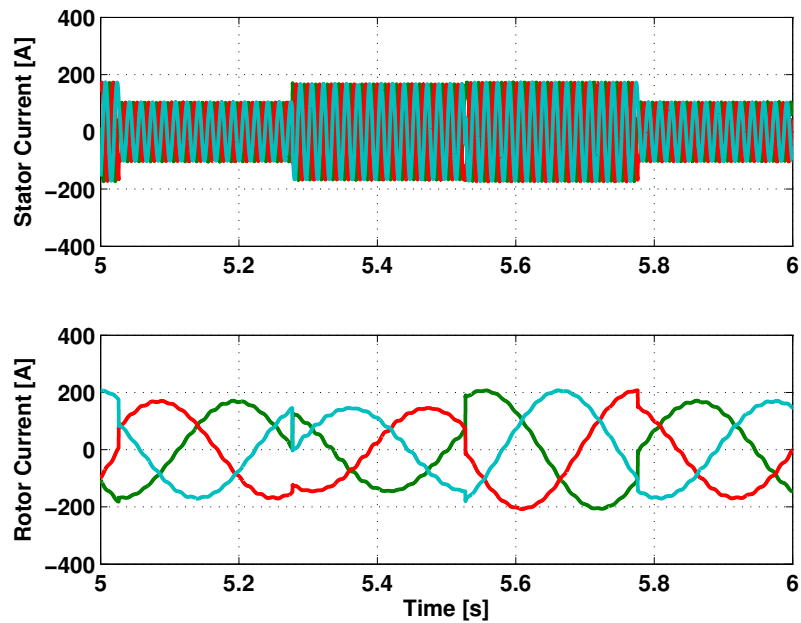

Figure 11. Stator and Rotor Currents using LDPC in a Flat Fading Channel.

To complete the analysis, it is presented in Fig. 12, a comparison of the BER performance for different values of E_b/N_0 for the proposed wireless coded neuro-fuzzy power control system using three different schemes: No Coding, CC, and LDPC. As expected, the performance of

LDPC is significantly superior than CC for flat fading channels. As pointed out in Fig. 12, for a BER of 10^{-5}, the performance improvement of LDPC over CC is approximately 26.8 dB and more than 30 dB over no coding. Table 1 shows a resume of the results presented in Fig. 12.
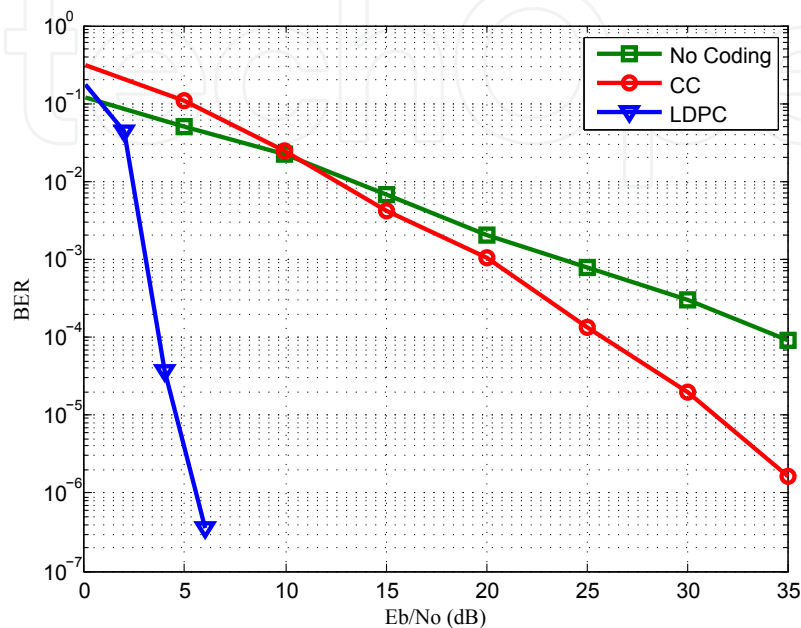

Figure 12. Performance Comparison for Different Coding Schemes in a Flat Fading Channel.

It can be seen that LDPC requires a significant lower E_b/N_0 to present the same order of performance of CC. It can be noted that, even for a low BER as 10^{-5}, it can occur some changes in the active and reactive power references that can cause serious problems in the generator, and consequentially, in the energy plant. However, the use of LDPC can reduce notably this number for a typical E_b/N_0 value and can improve considerably the system robustness to the channel impairments. For instance, a system operating with a typical E_b/N_0 of 10 dB employing CC will fail dramatically, while a system using LDPC coding will be free of errors.

Coding Scheme	Bit Error Rate	Eb/No (dB)
CC	10^{-3}	20.0
CC	10^{-4}	25.5
CC	10^{-5}	31.5
LDPC	10^{-3}	3.20
LDPC	10^{-4}	3.80
LDPC	10^{-5}	4.70

Table 1. Performance Comparison for Both Coding Schemes.

7. Conclusion

In this chapter, it was introduced a new wireless coded control system based on an adaptive neuro-fuzzy inference system applied to a doubly-fed induction aerogenerator. In order to improve the performance of the controller to the nonlinear characteristics of the wind system, the proposed adaptive neuro-fuzzy system uses a different design strategy based on the input and output data set collected from a DFIG with a deadbeat controller operating at different conditions and considering as input the rotor current error. The wireless communication system, employed to send the power reference signals to the DFIG controller, uses LDPC coding to reduce the transmission errors and the overall latency of the system by mitigating the necessity of retransmissions.

The presented analysis showed that the adaptive neuro-fuzzy strategy is a powerful technique to precisely control the dynamic nonlinear behavior of aerogenerators and to guarantee stability and maximum energy generation in smart grids applications. Furthermore, it was concluded that the use of LDPC coding can significantly improve the robustness of the wireless power control system in severe noise and fading channel conditions, being essential to maintain the integrity of the aerogenerators and to reduce the overall system response.

Appendix

Doubly-fed induction generator parameters [45]:

$R_1 = 24.75\ m\Omega$; $R_2 = 13.3\ m\Omega$; $L_M = 14.25\ mH$; $L_{l1} = 284\ \mu H$; $L_{l2} = 284\ \mu H$; $J = 2.6\ Kg \cdot m^2$; $N_P = 2$; $P_N = 149.2\ kVA$ and $V_N = 575\ V$.

Acknowledgments

Author details

I. R. S. Casella[1,*], A. J. Sguarezi Filho [1],
C. E. Capovilla [1], J. L. Azcue [2] and E. Ruppert [2]

* Address all correspondence to: ivan.casella@ufabc.edu.br; alfeu.sguarezi@ufabc.edu.br; carlos.capovilla@ufabc.edu.br; jl.azcue@gmail.com; ruppert@fee.unicamp.br

1 Centro de Engenharia, Modelagem e Ciências Sociais Aplicadas - CECS, Universidade Federal do ABC - UFABC, Brazil

2 Faculdade de Engenharia Elétrica e de Computação - FEEC, Universidade de Campinas - UNICAMP, Brazil

References

[1] M. Glinkowski, J. Hou, and G. Rackliffe. Advances in wind energy technologies in the context of smart grid. *Proceedings of the IEEE*, 99(6):1083–1097, June 2011.

[2] J. Wang, X. Du, and X. Zhang. Comparison of wind power generation interconnection technology standards. *Asia-Pacific Power and Energy Engineering Conference*, March 2011.

[3] W. Xiwen, Q. Xiaoyan, X. Jian, and L. Xingyuan. Reactive power optimization in smart grid with wind power generator. *Asia-Pacific Power and Energy Engineering Conference*, March 2010.

[4] J. F. Manwell, J. G. McGowan, and A. L. Rogers. *Wind Energy Explained: Theory, Design and Application*. Wiley, 2 edition, 2010.

[5] R. G. de Almeida and J. A. Pecas Lopes. Participation of doubly fed induction wind generators in system frequency regulation. *IEEE Transactions on Power Systems*, 22(3):944–950, August 2007.

[6] R. Datta and V. T. Rangathan. Variable-speed wind power generation using doubly fed wound rotor induction machine - a comparison with alternative schemes. *IEEE Trans. on Energy Conversion*, 17(3):414–421, September 2002.

[7] A. Tapia, G. Tapia, J. X. Ostolaza, and J. R. Saenz. Modeling and control of a wind turbine driven doubly fed induction generator. *IEEE Transactions on Energy Conversion*, 18(194-204), June 2003.

[8] S. A. Shaheen, H. M. Hasanien, and M. A. Badr. Study on doubly fed induction generator control. *International Middle East Power Systems Conference*, pages 627–633, 2010.

[9] Jin-Sung Kim, Jonghyun Jeon, and Hoon Heo. Design of adaptive pid for pitch control of large wind turbine generator. *International Conference on Environment and Electrical Engineering*, pages 1–4, 2011.

[10] B. Singh, E. Kyriakides, and S. N. Singh. Intelligent control of grid connected unified doubly-fed induction generator. In *IEEE Power and Energy Society General Meeting*, pages 1–7, July 2010.

[11] J.-S.R. Jang. Anfis: adaptive-network-based fuzzy inference system. *IEEE Transactions on Systems, Man, and Cybernetics*, 23(3):665–685, May-June 1993.

[12] M. Adamowicz, R. Strzelecki, Z. Krzeminski, J. Szewczyk, and L. Lademan. Application of wireless communication to small wecs with induction generator. *15th IEEE Mediterranean Electrotechnical Conference*, pages 944–948, June 2010.

[13] M. Adamowicz, R. Strzelecki, J. Szewczyk, and L. Lademan. Wireless short-range device for wind generators. *12th Biennial Baltic Electronics Conference*, pages 1736–3705, November 2010.

[14] T. J. Li. *Low complexity capacity approaching schemes: Design, analysis and applications*. Ph.D. dissertation, Texas AM Univ., 2002.

[15] J. G. Proakis. *Digital Communications*. MCGraw-Hill, 2008.

[16] H. Li, L. Lai, and W. Zhang. Communication requirement for reliable and secure state estimation and control in smart grid. *IEEE Transaction on Smart Grid*, 2(3):477–486, 2011.

[17] J. Jiang and K. R. Narayanan. Iterative soft decision decoding of reed solomon. *IEEE Communications Letters*, 8:244–246, 2004.

[18] S. Lin and D. J. Costello. *Error control coding*. Prentice Hall, 2004.

[19] C. Berrou, A. Glavieux, and P. Thitimajshima. Near shannon limit error-correcting coding and decoding: Turbo-codes. *IEEE International Communications Conference*, pages 1064–1070, 1993.

[20] J. Chen and A. Abedi. Distributed turbo coding and decoding for wireless sensor networks. *IEEE Communications Letters*, 15:166–168, 2011.

[21] I. R. S. Casella. Analysis of turbo coded ofdm systems employing space-frequency block code in double selective fading channels. *IEEE International Microwave and Optoelectronics Conference*, pages 516–520, November 2007.

[22] D. J. C. MacKay and R. M. Neal. Near shannon limit performance of low-density parity-check codes. *IET Electronics Letters*, 32:1645–1646, 1996.

[23] T. Richardson, A. Shokrollahi, and R. Urbanke. Design of capacity-approaching low-density parity-check codes. *IEEE Transactions on Information Theory*, 47:619–637, February 2001.

[24] IEEE. Standard for local and metropolitan area networks, part 16: Air interface for fixed and mobile wireless access systems. *IEEE Std. 802.16-2004*, 2004.

[25] A. J. Sguarezi Filho and E. Ruppert. A deadbeat active and reactive power control for doubly-fed induction generators. *Electric Power Components and Systems*, 38(5):592–602, 2010.

[26] W. Leonhard. *Control of Electrical Drives*. Springer-Verlag Berlin Heidelberg New York Tokyo, 1985.

[27] J.-S.R. Jang and C.-T. Sun. Neuro-fuzzy modeling and control. *Proceedings of the IEEE*, 83(3):378–406, March 1995.

[28] M. Sugeno and G. T. Kang. Structure identification of fuzzy model. *Fuzzy Sets and Systems*, 28, 1988.

[29] J. S. R. Jand, C.T. Sun, and E. Mizutani. *Neuro-Fuzzy and Soft Computing: A Computational Approach to Learning and Machine Intelligence*. Prentice Hall, 1997.

[30] S. Haykin. *Neural Networks: A Comprehensive Foundation*. Prentice Hall, 2 edition, 1998.

[31] P. Werbos. *Beyond regression: New tools for prediction and analysis in the behavioral sciences*. PhD thesis-Harvard University, 1974.

[32] R. G. Gallager. *Low-Density Parity-Check Codes*. Cambridge, 1963.

[33] Y. Zhang and W. E. Ryan. Toward low ldpc-code floors: a case stud. *IEEE Transactions on Communications*, 57(6):1566–1573, June 2009.

[34] R. M. Tanner. A recursive approach to low complexity codes. *IEEE Transactions on Information Theory*, 27(5):533–547, September 1981.

[35] H. Jin, A. Khandekar, and R. J. McEliece. Irregular repeat-accumulate codes. *Proc. Int. Symp. Turbo Codes and Related Topics*, pages 1–5, September 2000.

[36] M. Yang and W. E. Ryan. Lowering the error-rate floors of moderate length high-rate irregular ldpc codes. *Int. Symp. Information Theory*, 2:237, July 2003.

[37] M. Yang, W. E. Ryan, and Y. Li. Design of efficiently encodable moderate-length high-rate irregular ldpc codes. *IEEE Transactions on Communications*, 52(4):564–571, April 2004.

[38] Y. Zhang, W. E. Ryan, and Y. Li. Structured eira codes with low floors. *Proceedings of the International Symposium on Information Theory*, pages 174–178, September 2005.

[39] J. Kim, A. Ramamoorthy, and S. Mclaughlin. The design of efficiently-encodable rate-compatible ldpc codes. *IEEE Transactions on Communications*, 57:365–375, 2009.

[40] A. Barbieri, A. Piemontese, and G. Colavolpe. On the arma approximation for frequency-flat rayleigh fading channels. *IEEE International Symposium on Information Theory*, pages 1211–1215, June 2007.

[41] T. Richardson and R. Urbanke. The capacity of low-density parity check codes under message-passing decoding. *IEEE Transactions on Information Theory*, 47:599–618, February 2001.

[42] L. Dinoi, F. Sottile, and S. Benedetto. Design of versatile eira codes for parallel decoders. *IEEE Transactions on Communications*, 56(12):2060–2070, 2008.

[43] B. Shuval and I. Sason. On the universality of ldpc code ensembles under belief propagation and ml decoding. *IEEE 26th Convention of Electrical and Electronics Engineers*, pages 355–359, 2010.

[44] ETSI. Dvb-s.2. *Standard Specification*, pages 302–307, March 2005.

[45] A. J. Sguarezi Filho, M. E. de Oliveira Filho, and E. Ruppert. A predictive power control for wind energy. *IEEE Transactions on Sustainable Energy*, 2(1):97–105, January 2011.